5

Nonlinear Ellipsometry by Second Harmonic Generation

Fabio Antonio Bovino[1], Maria Cristina Larciprete[2], Concita Sibilia[2]
Maurizio Giardina[1], G. Váró[3] and C. Gergely[4]
[1]*Quantum Optics Lab Selex-Sistemi Integrati, Genova, Italy*
[2]*Department of Basic and Applied Sciences in Engineering, Sapienza University, Rome,*
[3]*Institute of Biophysics, Biological Research Center,*
Hungarian Academy of Sciences, Szeged,
[4]*Montpellier University, Charles Coulomb Laboratory UMR 5221, Montpellier,*
[1,2]*Italy*
[3]*Hungary*
[4]*France*

1. Introduction

Among the different nonlinear optical processes, second harmonic generation (SHG) is one of the most investigated. Briefly, polarization in a dielectric material can be expanded in terms of applied electric field. Second harmonic generation corresponds to an optical process of coherent radiation from electric-dipoles forming in the nonlinear optical material. In particular, SHG is related to the second term of the polarization expansion, thus it can be obtained only in materials which are noncentrosymmetric i.e. posses no centre of inversion symmetry. From the experimental point of view, the frequency of the incoming – fundamental- beam, ω, is doubled by the second order optical susceptibility $\chi_{ijk}^{(2)}$ of the material. The SHG processes, along with the structure of the nonlinear optical tensor, $\chi_{ijk}^{(2)}$, are strongly dependent on the crystalline structure of the material, thus by choosing the appropriate polarization state for the fundamental beam, different amplitude and polarization state of the nonlinear optical response can be selectively addressed.

As a consequence, several experimental techniques have been developed, for the determination of the different non-zero components of the third rank tensor $\chi_{ijk}^{(2)}$, with reference to a well-characterized sample. The Maker fringes technique (Maker et al, 1962), which is based on the investigation of oscillations of the SH intensity by changing the crystal thickness, has been without doubt the most employed. Briefly, this technique consists in measuring the SH signal transmitted trough the nonlinear crystal as a function of the fundamental beam incidence angle, which is continuously varied by placing the sample onto a rotation stage. The polarization states of both fundamental and generated beams are selected by rotating a half-wave plate (polarizer) and a linear polarizer (analyzer), respectively. On a reference line, a small fraction of the fundamental beam is usually sent onto a reference crystal, which is hold at a fixed incidence angle, in order to minimize the influence of laser energy fluctuations. On the measurement line, the second harmonic signal

is detected with a photomultiplier, while interference and dichroic filters are used to suppress the fundamental beam.

Second harmonic signal can also be generated at a surface, being itself responsible for a symmetry break (Bloembergen et al, 1968). When looking for surface contributions to the SH signal, rather than bulk contribution, the reflective second harmonic generation (RSHG) technique has to be employed. This technique involves the detection of the reflected SH signal, at a fixed incidence angle of the pump beam, while sample is rotated along its surface normal. Specifically, depending on the form of the bulk $\chi_{ijk}^{(2)}$ tensor, there may be some particular combinations of the polarization states of fundamental and generated beams may inhibit the bulk induced SHG. As a consequence, any signal measured in these polarizations combinations would be ascribed to surface effects.

The noncollinear scheme of SHG experiments was firstly introduced by Muenchausen (Muenchausen et al, 1987) and Provencher (Provencher et al, 1993) and, since then, it was exploited more recently by different authors. It presents some advantages, with respect to conventional collinear SHG, as a reduced coherence length (Faccio et al, 2000) as well as the possibility to distinguish between bulk and surface responses (Cattaneo & Kauranen, 2005) thus this technique represents a promising tool for surface and thin-film characterization (Cattaneo & Kauranen, 2003).

Very recently, we developed a method, based on the noncollinear scheme of SHG, to evaluate the non-zero elements of the nonlinear optical susceptibility. At a fixed incidence angle, the generated noncollinear SH signal is investigated while continuously varying the polarization state of *both* fundamental beams. The obtained experimental results show the peculiarity of the nonlinear optical response associated with the noncollinear excitation, and can be fully explained using the expression for the effective second order optical nonlinearity in noncollinear scheme. The resulting *polarization chart*, recorded for a given polarization state of the SH signal, shows pattern which is characteristic of the investigated crystalline structure. It offers the possibility to evaluate the ratio between the different non-zero elements of the nonlinear optical tensor. Moreover, if the measurements are performed with reference to a well-characterized sample, i.e. a nonlinear optical crystal as quartz or KDP, this method allows the evaluation of the absolute values of the non-zero terms of the nonlinear optical tensor, without requiring sample rotation. As a consequence, this technique turns out to be particularly appropriate for those experimental conditions where the generated SH signal can be strongly affected by sample rotation angle. For instance, if a sample is some coherence lengths thick, as the optical path length is changed by rotation, the SH signal strongly oscillates with increasing incidence angle (Jerphagnon & Kurtz, 1970) according to Maker-fringes pattern, thus a high angle resolution would be required. When using short laser pulses, whose bandwidth is comparable or lower than sample thickness, as the incidence angle is modified the nonlinear interaction may involve different part of the sample and, eventually, surface contributions. For nano-patterned samples, finally, a rotation would imply differences into sample surface interested by the pump spot size. With respect to the mentioned examples, the method of polarization scan simplifies the characterization of the nonlinear optical tensor elements without varying the experimental conditions, and turns out to be a sort of *nonlinear ellissometry*.

In what follows, we will describe in details some applications that we recently developed, where the polarization mapping is employed for the characterization of some nonlinear

optical materials as gallium nitride (GaN), zinc oxide (ZnO) and, more specifically to Bacteriorhodopsin films.

2. Evaluation of the non-zero elements of the $\chi^{(2)}$ tensor components

As far as noncollinear SHG is concerned, as in our recent works, the number of experimental parameters which can be combined, so to determine the polarization and amplitude of the SH signal, is increased. As a matter of fact, the two pump beams, tuned at $\omega_1=\omega_2$, having different incidence angles, α_1 an α_2, and polarization state, ϕ_1 and ϕ_2, cooperate in the determination, and thus in the excitation, of the nonlinear optical polarization, $P^{(2)}=\chi^{(2)}:E_1(\omega_1)E_2(\omega_2)$.

We successfully tested this kind of nonlinear ellisometry onto a Gallium nitride slab, 302 nm thick, grown by metal-organic chemical vapour deposition (MOCVD) onto (0001) c-plane Al2O3 substrates (Potì et al, 2006). GaN presents a wurtzite crystal structure without centre of inversion, thus leading to efficient second order nonlinear effects (Miragliotta et al, 1993). In addition, the wide transparency range, which extends form IR to the near UV, make this material extremely appealing from nonlinear optical point of view.

We employed the output of a mode-locked femtosecond Ti:Sapphire laser system tuned at λ=830 nm (76 MHz repetition rate, 130 fs pulse width), which was split into two beams of about the same intensity. The polarization state of both beams (ϕ_1 and ϕ_2) was varied with two identical half wave plates, automatically rotating, that were carefully checked not to give nonlinear contribution. Two collimating lenses, 150 mm focal length, were placed thereafter, while the sample was placed onto a motorized combined translation and rotation stage which allowed the variation of the rotation angle, α, with a resolution of 0.5 degrees. The temporal overlap of the incident pulses was automatically controlled with an external delay line. Several details of the experimental scheme are given in Fig. 1.

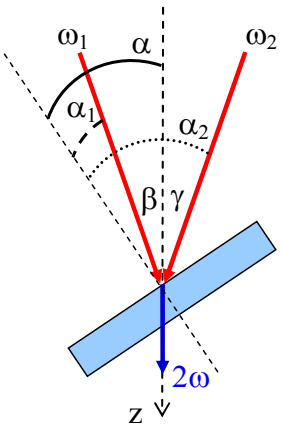

Fig. 1. Sketch of the noncollinear scheme adopted for second harmonic generation measurements. For a fixed sample rotation angle α, measured with respect to the z-axis, the corresponding incidence angles of the two pump beams result to be $\alpha_1=\alpha-\beta$ and $\alpha_2=\alpha-\gamma$, respectively.

In the experiments reported in (Larciprete et al, 2009) the sample rotation angle was fixed to α=35°, while the pump beams were sent to intersect in the focus region with the angles β=9° and γ= -9° , i.e. the corresponding incidence angles of the two pump beams onto the sample result to be $\alpha_1=\alpha-\beta$ and $\alpha_2=\alpha-\gamma$, respectively.

GaN crystal structure, i.e. wurtzite, is characteristic of III-V nitrides and presents the noncentrosymmetric point group symmetry 6mm with a hexagonal primary cell. The only nonvanishing second order susceptibility tensor elements (J.Chen, Z.H.Levine, J.W.Wilkins, Appl. Phys. Lett. 66, pp. 1129-1131 (1995)) are $\chi_{311}^{(2)} = \chi_{322}^{(2)}$, $\chi_{333}^{(2)}$, and $\chi_{113}^{(2)} = \chi_{131}^{(2)} = \chi_{223}^{(2)} = \chi_{232}^{(2)}$, which correspond to $\chi_{15}^{(2)}=\chi_{24}^{(2)}$, $\chi_{31}^{(2)}=\chi_{32}^{(2)}$ and $\chi_{33}^{(2)}$, referring to the piezoelectric contraction, or equivalently, being $\tilde{d}_{ij}=\frac{1}{2}\tilde{\chi}_{ij}^{(2)}$ the second order nonlinear optical tensor can be written as follows:

$$\tilde{d}=\begin{pmatrix} 0 & 0 & 0 & 0 & d_{15} & 0 \\ 0 & 0 & 0 & d_{24} & 0 & 0 \\ d_{31} & d_{32} & d_{33} & 0 & 0 & 0 \end{pmatrix} \tag{1}$$

The five non-zero terms further reduce to three independent coefficients in wavelength regimes where it is possible to take advantage of Kleinmann symmetry rules, i.e. $d_{15}=d_{24}=d_{31}=d_{32}$ and $d_{33}= -2\cdot d_{31}= -2\cdot d_{15}$.

Given the tensor (1), by selecting the appropriate polarization state for the two fundamental beams, it is possible to address the different non-zero components of $d_{ij}^{(2)}$ and, consequently, to get different polarization state for the generated signal.

The full expression of the SH power, $W_{\omega1+\omega2}$, as a function of sample rotation angle α, is given by:

$$W_{\omega1+\omega2}(\alpha)=\left(\frac{512\pi^3}{A_1A_2}\right)(t_{\omega1})^2\cdot(t_{\omega2})^2\cdot T_{\omega1+\omega1}\cdot W_{\omega1}\cdot W_{\omega2}\frac{\sin^2\left(\Psi_{SHG}(\alpha)\right)}{\left[n_{\omega1}\cdot n_{\omega2}-n^2{}_{\omega1+\omega2}\right]^2}\left(d_{eff}(\alpha)\right)^2 \tag{2}$$

where A_1 and A_2 are the fundamental beams transverse areas onto sample surface, retrieved from the main beam area (A), $W_{\omega1}$ and $W_{\omega2}$ are the power of the incident fundamental beams. The Fresnel transmission coefficients for the two fundamental fields at the input interfaces are $t_{\omega1}(\alpha_1,\phi_1)$ and $t_{\omega2}(\alpha_2,\phi_2)$, while $T_{\omega1+\omega2}(\alpha,\phi)$ is the Fresnel transmission coefficient for the SH power at the output interface. As far as material optical birefringence is concerned, Fresnel coefficients and refractive indices of both fundamental and generated beams, i.e. $n_{\omega1}(\alpha'_1,\phi_1)$, $n_{\omega2}(\alpha'_2,\phi_2)$ and $n_{\omega1+\omega2}(\alpha'_{\omega1+\omega2},\phi)$ are dependent on the propagation angle and polarization state of the respective beam.

Finally, Ψ_{SHG} is the phase factor given by:

$$\Psi_{SHG}=\left(\frac{\pi L}{2}\right)\left(\frac{2}{\lambda}\right)\left[n_{\omega1}\cdot\cos(\alpha'_{\omega1})+n_{\omega2}\cdot\cos(\alpha'_{\omega2})-2n_{\omega1+\omega2}\cdot\cos(\alpha'_{\omega1+\omega2})\right], \tag{3}$$

where L is sample thickness.

The analytical expression of the effective nonlinear susceptibility, $d_{eff}(\alpha)$ can be rather complicated, being dependent on the tensor components, the polarization state of the three electric fields and, of course, on the fundamental beams incidence angles. However, for point group symmetry 6mm, as in the case of GaN, the final expressions for $d_{eff}(\alpha)$, as a function of polarization angle of the two pumps, becomes:

$$d_{eff}^{\hat{s}} = -d_{15}\left[\sin(\phi_1)\cos(\phi_2)\sin(\alpha'_2) + \cos(\phi_1)\sin(\phi_2)\sin(\alpha'_1)\right]$$

$$\begin{aligned} d_{eff}^{\hat{p}} = &-d_{24}\cos(\alpha)\left[\cos(\alpha'_1)\sin(\alpha'_2) + \sin(\alpha'_1)\cos(\alpha'_2)\right]\cos(\phi_1)\cos(\phi_2) - \\ &-\sin(\alpha)\left\{d_{31}\sin(\varphi_1)\sin(\varphi_2) + \cos(\phi_1)\cos(\phi_2)\left[d_{32}\cos(\alpha'_1)\cos(\alpha'_2) + d_{33}\sin(\alpha'_1)\sin(\alpha'_2)\right]\right\} \end{aligned} \quad (4)$$

where the apex stands for the polarization state of the generated beam and α'_1, α'_2 are the internal propagation angles of the two pump beams inside the sample. Equations (4) quite completely and exhaustively describe the interaction of two incident pump beams linearly polarized with a noncentrosymmetric material presenting GaN crystalline structure. For any other generic polarization angle of the SH beam, ϕ, the $d_{eff}(\alpha)$ results in a combination of terms given by the Eeq.(4): $d_{eff}^{\phi} = \sin(\phi)\, d_{eff}^{\hat{s}} + \cos(\phi)\, d_{eff}^{\hat{p}}$.

Following these considerations, we measured the generated signal as a function of the polarization state of both pump beams, at three different sample rotation angles, i.e. for α=35 , 9 nd 1 degrees. The two half-wave plates were systematically rotated, in the range -180 -+180 degrees for the first pump beam (ϕ_1) and 0 -180 degrees for the second pump beam (ϕ_2).

We show the obtained measurements in Fig.2.a and Fig.2.b for the two different polarization state of the analyzer, namely $\hat{p}$ ϕ_1=0°, and $\hat{s}$, ϕ_2=90°, respectively. Considering the $\hat{p}$ -polarized SH signal (Fig.2.a) it can be seen that the absolute maxima are achievable when both pumps are $\hat{p}$ -polarized, i.e. when ϕ_1 and ϕ_2 are both 0° or 180°, while relative maxima occur when both pumps are $\hat{s}$ -polarized, i.e. when polarization angles of both pumps are set to ± 90°. Conversely, when the two pump beams have crossed polarization, i.e when ϕ_1=0° and ϕ_2=90° and viceversa, the nonlinear optical tensor of GaN do not allow second harmonic signal which is $\hat{p}$ -polarized thus the corresponding measurements go to zero.

A fairly different behavior is observable, when the analyzer is set to $\hat{s}$ -polarization, i.e. ϕ=90° (see Fig.2.b). In this case, the maxima generally occur when the two pump beams have crossed polarization, but since this condition is no more symmetrical for positive and negative rotation angles, the resulting surface plots present some variation at different rotation angles. When α=35° (Fig.2.b), the absolute maxima take place when the first pump is $\hat{s}$ -polarized and the second pump is $\hat{p}$ -polarized, i.e. ϕ_1= ±90° and ϕ_2 is equal to either 0° or 180°. Relative maxima occur in the reverse situation, when the first pump is $\hat{p}$ -polarized, ϕ_1=0° or ±180°, and the second pump $\hat{s}$ -polarized, ϕ_2=90°. Finally, if the two pumps are equally polarized, either $\hat{s}$ or $\hat{p}$, the generation of $\hat{s}$ -polarized signal is not allowed.

The calculated polarization charts, reported in Fig.3.a and Fig.3.b, were retrieved from Equations (4) by assuming the Kleinmann symmetry rules for the nonlinear optical tensor elements.

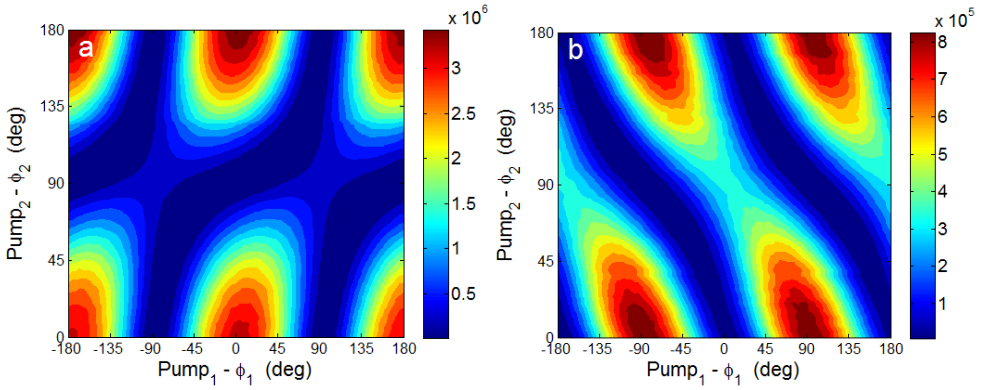

Fig. 2. Noncollinear second harmonic signal experimentally measured as a function of the polarization state of the first pump beam (ϕ_1) and the second pump beam (ϕ_2). Sample rotation angle was fixed to α=35° . The polarization state of the analyzer is set to (a) $\hat{p}$ i.e. ϕ=0° and (b) $\hat{s}$, i.e. ϕ=90°.

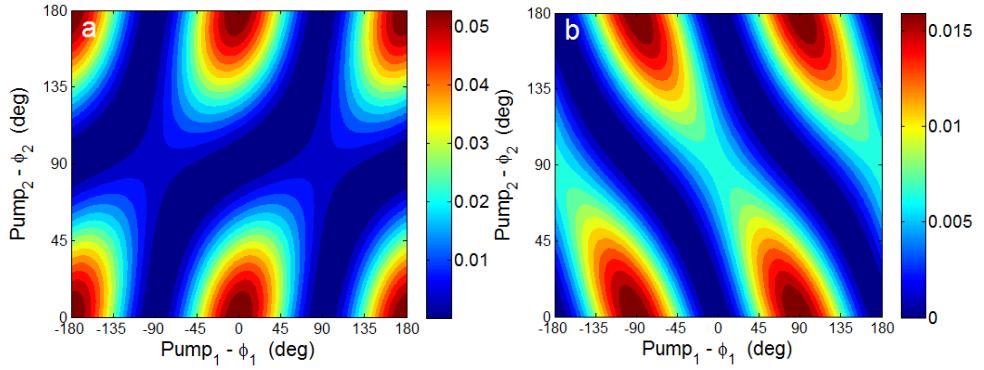

Fig. 3. Noncollinear second harmonic signal theoretically calculated as a function of the polarization state of the first pump beam (ϕ_1) and the second pump beam (ϕ_2). Sample rotation angle was fixed to α=35°. The polarization state of the analyzer is set to (a) $\hat{p}$ i.e. ϕ=0° and (b) $\hat{s}$, i.e. ϕ=90°.

The perfect matching between the experimental and theoretical charts verify the rightness of the symmetry assumption. Assuming a different relationship between the coefficients d_{15}, d_{31} and d_{33} would in fact lead to evident changes in the polarization charts.

In order to evaluate the effect of sample rotation angle, we performed further experimental measurements at different sample rotation angles. The experimental plots obtained for α=1° and 9° are shown in Fig.4 and Fig.5, respectively.

The polarization charts of the noncollinear SH signal generated in $\hat{p}$ polarization (see Fig.4.a and Fig.5.a) display a similar symmetry at all the sample rotation angles, while amplitude is decreasing with decreasing rotation angle.

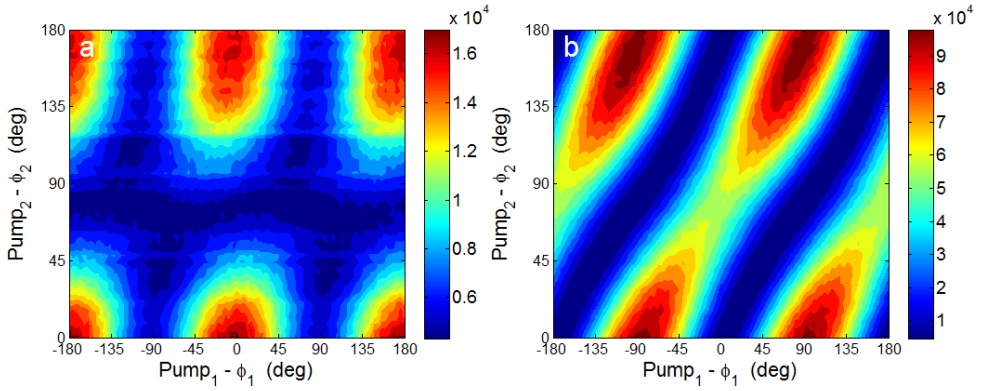

Fig. 4. Noncollinear second harmonic signal experimentally measured as a function of the polarization state of the first pump beam (ϕ_1) and the second pump beam (ϕ_2). Sample rotation angle was fixed to α=1°. The polarization state of the analyzer is set to (a) $\hat{p}$ i.e. ϕ=0° and (b) $\hat{s}$, i.e. ϕ=90° .

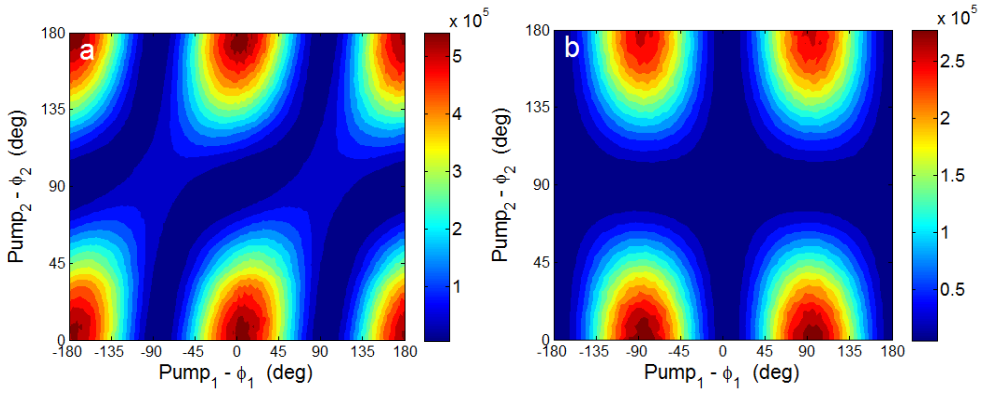

Fig. 5. Noncollinear second harmonic signal experimentally measured as a function of the polarization state of the first pump beam (ϕ_1) and the second pump beam (ϕ_2). Sample rotation angle was fixed to α=9°. The polarization state of the analyzer is set to (a) $\hat{p}$ i.e. ϕ=0° and (b) $\hat{s}$, i.e. ϕ=90°.

On the other side, the $\hat{s}$ -polarized SH signal (see Fig.4.b and Fi.5.b), according with the theoretical model, result in a modified trend of both the Fresnell coefficients and the effective nonlinearity as a function of ϕ_1 and ϕ_2. As a consequence, when the rotation angle α is set to 1° (Fig.4.b) we found that the plots appear to be reversed, with respect to α =35°.

Curiously, when α =9° the same conditions hold for the absolute maxima and for the zero signal, while the relative maxima disappeared. This unusual behavior can be explained considering that fixing the sample rotation angle to 9°, i.e. fixing $\alpha=\beta$, corresponds to a situation such that the first pump beam is normally incident onto the sample. For an anisotropic uniaxial crystal with the optical axis perpendicular to sample surface, as the

investigated GaN film, a normally incident wave always experiences the ordinary refractive index, whatever its polarization angle. Thus, from the refractive index point of view, the polarization state of the first pump beam always corresponds to the case of $\hat{s}$-polarization. As a consequence, the condition to get the relative maxima, i.e. the first pump $\hat{p}$-polarized and the second pump $\hat{s}$-polarized, is never fulfilled, since it is replaced with the combination of two pumps both having $\hat{s}$-polarization and the SH generation of $\hat{s}$-polarized signal is prohibited. As we will show in the next section, this experimental configuration, i.e. one of the pump is normally incident onto the sample, is particularly suited to put evidence a tilt in the optical axis, since it would result in a modified pattern of the $\hat{s}$ polarized signal.

Finally, we have shown that the *polarization charts* offer all the information to evaluate the ratio between the different non-zero elements of the nonlinear optical tensor, thus verifying if Kleinman's symmetry rules can be applied to a given material. The method we have described is an extension of Maker fringes technique to the noncollinear case and represents a useful tool to characterize the non-zero terms of the nonlinear optical tensor without varying relevant experimental conditions as incidence angles.

3. Evaluation of the optical axis tilt of Zinc oxide films

We applied the noncollinear nonlinear ellissometry to ZnO films grown by dual ion beam sputtering and show that the proposed nonlinear ellissometry is an useful tool to put into evidence a tilt angle of the optical axis of a nonlinear optical film with respect to the surface normal, for any material whose symmetry class implies an orientation of the optical axis almost perpendicular to the surface (Bovino et al, 2009).

Zinc Oxide was chosen for the large energy gap value (Eg = 3.37 eV) and high nonlinear optical coefficients, of both second and third order, it offers (Blachnik et al, 1999). Second order nonlinear optical response has been shown in ZnO films grown by different techniques implying both high deposition temperature (as reactive sputtering, spray pyrolysis, laser ablation) and low deposition temperature (as laser deposition, and dual ion beam sputtering). Generally, the reduced deposition temperature results in polycrystalline films, where the average orientation of crystalline grains, along with the resulting optical axis, can be tilted with respect to the ideal crystal, i.e. normal to sample surface.

Zinc oxide films, 400 nm thick, were deposited by means of a dual ion beam sputtering system onto silica substrates. Preliminary X-ray diffraction investigation performed on the obtained films indicate that the films are polycrystalline with the c-axis preferentially oriented about the surface normal (Weißenrieder & Muller, 1997).

As well as for GaN, ZnO crystalline structure belongs to the noncentrosymmetric point group symmetry 6mm with a hexagonal primary cell, thus the non-zero components are the same, i.e. $d_{15}=d_{24}=d_{31}=d_{32}$ and $d_{33}= -2\cdot d_{31}= - 2 \cdot d_{15}$, under Kleinmann's approximation. However, it must be pointed out that this assumption holds only if the optical axis is normal to the sample surface. If, on the other hand, the optical axis is somehow tilted, with respect to the surface normal, a rotation must be introduced into the expression of the nonlinear optical tensor, that in turns results into the introduction of other nonvanishing terms in the effective nonlinear susceptibility.

The analytical expression of the effective susceptibility, $d_{eff}(\alpha)$, for the ZnO crystalline structure, considering four combination of polarization states of the two pump beams, $\hat{p}_{\omega 1}-\hat{p}_{\omega 2}$, $\hat{s}_{\omega 1}-\hat{s}_{\omega 2}$, $\hat{p}_{\omega 1}-\hat{s}_{\omega 2}$ and $\hat{s}_{\omega 1}-\hat{p}_{\omega 2}$, four different expressions for $d_{eff}(\alpha)$ are allowed, depending on the SH polarization state, i.e. either $\hat{p}$ or $\hat{s}$:

$$
\begin{aligned}
d_{eff}^{pp\to p} &= -\cos(\alpha_{2\omega})d_{24}\left[\cos(\alpha_1^{'})\sin(\alpha_2^{'})+\cos(\alpha_2^{'})\sin(\alpha_1^{'})\right]+ \\
&+\sin(\alpha_{2\omega})\left[-d_{32}\cos(\alpha_1^{'})\cos(\alpha_2^{'})-d_{33}\sin(\alpha_2^{'})\sin(\alpha_1^{'})\right] \\
d_{eff}^{ss\to p} &= -\sin(\alpha_{2\omega})d_{31} \\
d_{eff}^{ps\to s} &= -d_{15}\sin(\alpha_1^{'}) \\
d_{eff}^{sp\to s} &= -d_{15}\sin(\alpha_2^{'})
\end{aligned}
\tag{5}
$$

Where α'_1, α'_2 are the internal propagation angles of the two pump beams inside the sample, and $\alpha_{2\omega}$ is the angle of emission of the SHG inside the crystal.

Referring to Fig.1, the two pump beams were sent to intersect in the focus region with the angles β= 9° and γ= -9° , while α was fixed to 9°. As a matter of fact, the fundamental beam 1 was normally incident onto the sample. The experimental measurements were obtained by rotating the two half-wave plates, in the range -180° -+180° for pump beam 1 and 0° -180° for pump beam 2.

The experimental plots, obtained when the analyzer was set to $\hat{s}$ -polarization, are shown in Figure 6.a. As we already mentioned in the previous section, the maxima of SH signal should occur when the two pump beams have crossed polarization. However, in this particular condition, the absolute maxima still require $\hat{s}$ -polarization for pump 1 and $\hat{p}$ -polarization for pump 2 (i.e. ϕ_1= ± 90 and ϕ_2 equal to either 0 or 180), whereas the relative maxima totally disappeared. In this configuration, in fact, the pump beam 1 is normally incident onto the sample (see Figure 6.b) thus it is always $\hat{s}$ -polarized, i.e. the condition to get a relative maximum ($\hat{p}$ -polarization for pump 1 and $\hat{s}$ -polarization for pump 2) vanishes. What is even more interesting, we found out that the experimental configuration where one of the pump beams is normally incident onto the sample, is particularly sensitive to the orientation of the optical axis.

The experimental curves were fully reconstructed using the expression for the effective second order optical nonlinearity in noncollinear scheme, assuming the Kleinmann symmetry rules. Dispersion of both the ordinary and extraordinary refractive indices of ZnO are taken from reference (Figliozzi et al, 2005).

We show in Fig.7.a the calculated curve for α=9°, when the optical axis is assumed to be perpendicular to sample surface. If compared with the theoretical one, the experimental curve appears to be shifted towards higher ϕ_2. This difference between experimental and theoretical curves suggest that the optical axis may be averagely tilted with respect to the surface normal. From the point of view of the investigated ZnO film, this is a reasonable assumption, taking into account the low temperature deposition technique which was employed. In order to fit the experimental data, an angular tilt of the optical axis was then

introduced in the analytical model through a rotation matrix, applied on the $d_{eff}(\alpha)$. This rotation produces the arising of some new terms in the nonlinear optical tensor. In Fig. 7.b we show the polarization chart calculated in this way, assuming a tilt of only 2 around the x-axis, as shown in Fig.8.

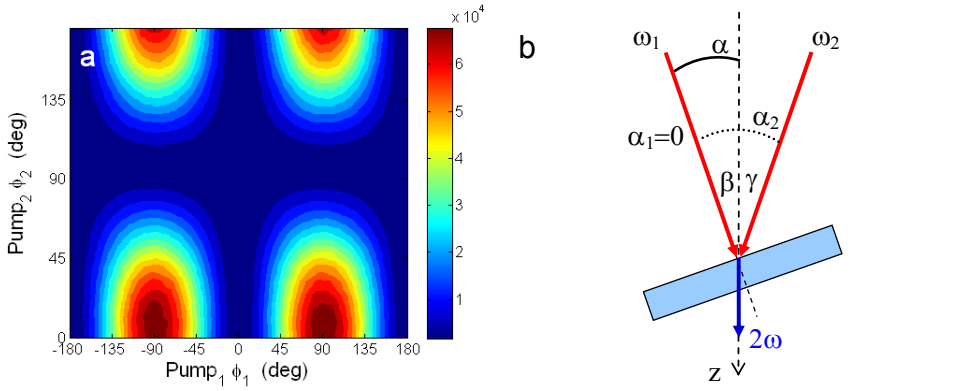

Fig. 6. (a) Noncollinear SH signal measured as a function of the polarization state of the first pump beam (ϕ_1) and the second pump beam (ϕ_2).The polarization state of the analyzer is set to $\hat{s}$, i.e. ϕ=90°. (b) Sketch of the experimental configuration: sample rotation angle was fixed to α=9°.

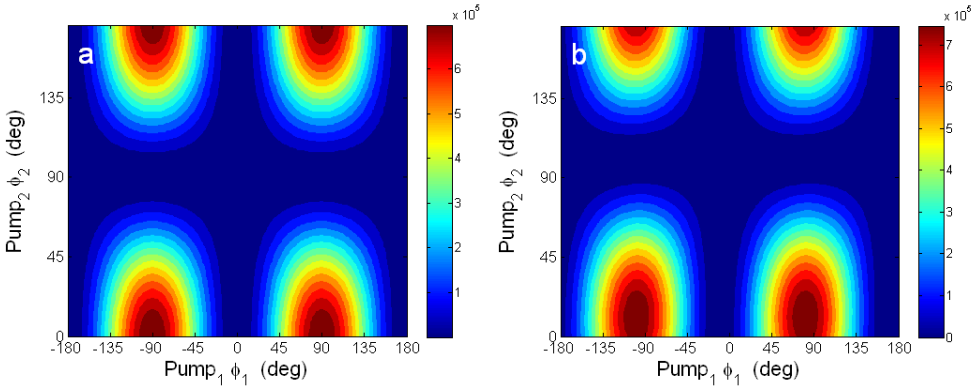

Fig. 7. Theoretically calculated curves of $\hat{s}$ -polarized second harmonic signal as a function of the polarization angle of the first pump beam (ϕ_1) and the second pump beam (ϕ_2), calculated for the optical axis (a) normal to the sample surface and (b) tilted about the x-axis of 2 degrees. Sample rotation angle is α= 9° .

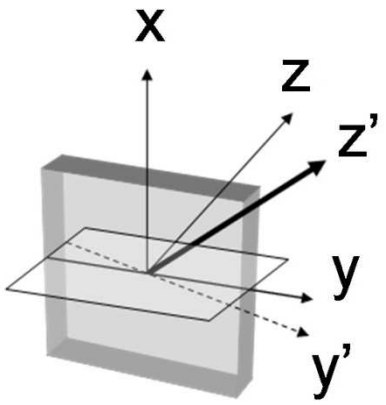

Fig. 8. Sketch of the film orientation. z and z' represents the optical axis orientation before and after rotation about the x-axis, respectively.

The obtained theoretical curve displays the same ϕ_Z-shift evidenced in the experimental curves, thus confirming that the film has a partially oriented polycrystalline structure, as also shown by the X-ray analysis, but the orientation of the optical axis is not exactly normal to the film surface. Similar curves were calculated by tilting the optical axis, along with the nonlinear optical tensor, around the other two reference axes. It's worth to note that for the investigated crystalline symmetry group, 6mm, a rotation about the z-axis does not produce any change in the nonlinear optical tensor. On the other side, a rotation about the y-axis produce an analogous shift in the $\hat{s}$ -polarized SH pattern, but also a modification in the $\hat{p}$ -polarized SH pattern which was not compatible with the corresponding experimental curves.

We conclude, from the experimental results obtained from ZnO films deposited by dual ion beam sputtering, that the *polarization chart* of the noncollinear SH signal can provide important information on the crystalline structure of the films. Specifically, the polarization scanning method adopted is a valid and sensitive tool to probe the orientation of the optical axis and to evidence possible angular tilt with respect to surface normal.

4. Application of the nonlinear ellisometry to Bacteriorhodopsin films

We recently extended the use of the nonlinear ellisometry to the study of chiral molecules, i.e. those molecules lacking an internal plane of symmetry thus having a non-superimposable mirror image. SHG processes have been extensively used for the characterization of optical chirality, due to the large obtainable effects, with respect to conventional linear optical techniques. Considering the nonlinear optical tensor, in fact, the optical chirality is responsible for the introduction of the so-called chiral components. The study of optical chirality by means of SHG was first introduced by Petralli-Mallow and co-workers from a circularly polarized fundamental beam (Petralli-Mallow et al, 1993). Later on, it was demonstrated that also a linearly polarized fundamental beam can be employed to discern chiral components of the nonlinear optical tensor (Verbiest et al, 1995). More recently, a new technique, based on the use of focused laser beams at normal incidence, was applied (Huttunen et al, 2009) to avoid the coupling of possible anisotropy of the sample and thus spurious signals.

The chiral molecule we investigated is Bacteriorhodopsin (BR), a trans-membrane protein found in purple membrane patches in the cell membrane of Halobacterium salinarium, a naturally occurring archaeon in salt marshes. BR proteins naturally arrange in trimers to form a hexagonal two-dimensional lattice in the purple membrane, as shown in Fig.9.a, acting as a natural photonic band gap material (Clays et al, 1993). Furthermore, each BR monomer contains a covalently bound retinal chromophore, presenting its own transition dipole, which is responsible for its outstanding nonlinear optical response (Verbiest et al, 1994) as well as for optical chirality (Volkov et al, 1997).

We examined a 4 μm thick BR film, deposited via an electrophoretic deposition technique onto a substrate covered by a 60 nm thick ITO film. In the resulting BR film, composed by ~800 purple membrane layers (of 5nm thickness each), the chromophore retinal axis is oriented at an angle of 23 ± 4° with respect to the plane of the purple membrane (Schmidt & Rayfield, 1994), i.e. forming an isotropic conical polar distribution around the normal, as shown in Figure 9.b.

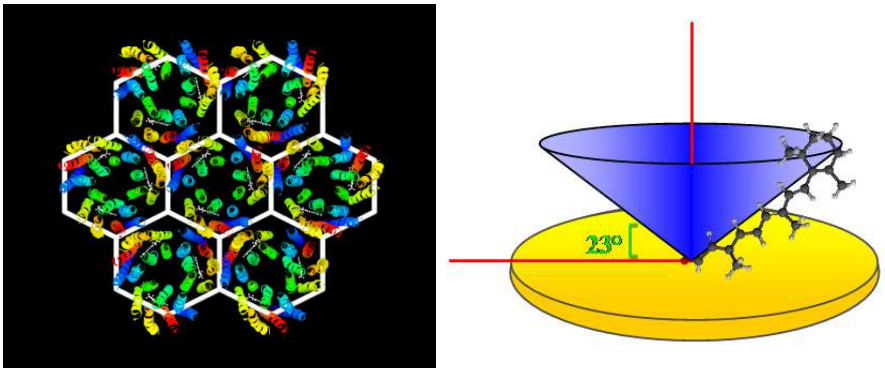

Fig. 9. (a) Hexagonal two-dimensional lattice of BR proteins trimers', as naturally arrange in the purple membrane. (b) Orientation of the retinal chromophores, forming a cone around the normal to the membrane plane, at an angle of 23± 4° relative to the membrane plane.

The BR symmetry structure, arising by consecutive stacking of the naturally hexagonal lattice represented by the membrane sheets having P3 symmetry is noncentrosymmetric, thus its second order susceptibility tensor has three nonvanishing components, i.e. $d_{15}=d_{24}$, $d_{31}=d_{32}$ and d_{33}. Two additional nonzero components of the nonlinear susceptibility tensor, $d_{14}= -d_{25}$, determine the so-called chiral contribution to the nonlinear optical response, since they appear only if molecules have no planes of symmetry (Hecht & Barron, 1996). As a result, the nonlinear optical tensor turns out to be:

$$\tilde{d} = \begin{pmatrix} 0 & 0 & 0 & d_{14} & d_{15} & 0 \\ 0 & 0 & 0 & d_{24} & d_{25} & 0 \\ d_{31} & d_{32} & d_{33} & 0 & 0 & 0 \end{pmatrix} \tag{6}$$

Experimental investigation of the noncollinear SH signal, was performed with the two pump beams angles set to $\beta = 3°$ and $\gamma = -3°$, respectively, while α was fixed to -40° . The polarization state of both pump beams was systematically varied in the range -90° -+90°. Measurements corresponding to $\hat{p}$ - and $\hat{s}$ -polarized SH are shown in Fig.10.

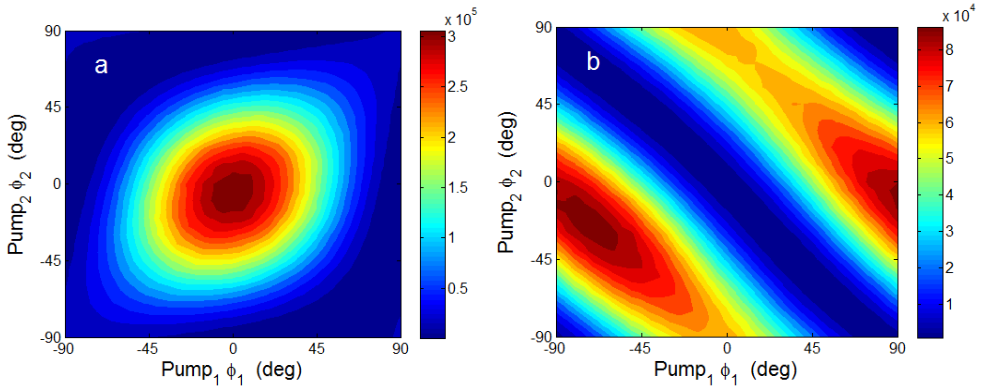

Fig. 10. (a) Noncollinear second harmonic signal experimentally measured as a function of the polarization state of the first pump beam (ϕ_1) and the second pump beam (ϕ_2). Sample rotation angle was fixed to α= -40°. The polarization state of the analyzer is set to (a) $\hat{p}$ i.e. ϕ=0° and (b) $\hat{s}$, i.e. ϕ=90°.

The obtained experimental results indicate that it is possible to retrieve important information also about the optical chirality of the sample from the polarization charts, and in particular from the $\hat{p}$ -polarized signal. In fact, considering the $\hat{p}$ -polarized signal (Figure 10.a) in absence of optical chirality the maximum signal would be located in correspondence of ϕ_1=ϕ_2=0° , i.e. when both pumps are $\hat{p}$ -polarized. In contrast, the pattern shown in Fig.10.a presents a maximum that is somewhat shifted towards the negative quadrant, i.e. both ϕ_1 and ϕ_2 are <0 . It's worth to note that a small value of the chiral components, as can be for instance $|d_{14}| = |d_{25}| = 0.1 \cdot d_{33}$ (Larciprete et al, 2010), still determines an observable effect onto the polarization chart. In Fig.11 the central area of

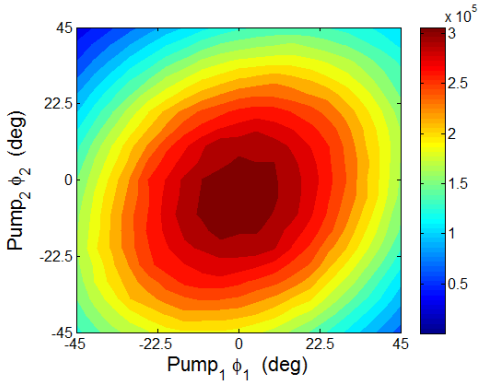

Fig. 11. Detail of the noncollinear second harmonic signal experimentally measured as a function of the polarization state of both pump beams, i.e. ϕ_1 and ϕ_2. Sample rotation angle was α= -40° . The polarization state of the analyzer is set to $\hat{p}$ i.e. ϕ=0°.

Fig.10.a. has been magnified, in order to appreciate the described effect. On the other hand, it must be said that for achiral structures, being $d_{14}=d_{25}= 0$ the resulting polarization chart would show a maximum signal well-centred onto the axis' origin.

Finally, from further experimental measurements, performed by changing other parameters as for instance pump beams' power, we trust to put in evidence the role of different potential sources of the nonlinear polarization and in particular the nonlinear magnetic one. This part of the work is still in progress and thus it will be accurately described elsewhere.

5. Conclusion

In conclusion, we developed a method, based on the detection of noncollinear SHG by continuously varying the polarization state of *both* the fundamental beams within a certain range. We have shown that the resulting *polarization charts*, that can be recorded for a given polarization state of the SH signal, present a typical pattern being a signature of a characteristic crystalline structure. First of all, this kind of nonlinear ellipsometry, that doesn't require sample rotation, offers the possibility to evaluate the ratio between the different non-zero elements of the nonlinear optical tensor, or even their absolute values. Furthermore, it represents a valid and sensitive tool to investigate the orientation of the optical axis of a given crystalline structure, being able to evidence possible angular tilt with respect to surface normal. Finally, the polarization scanning method adopted is also able to put in evidence optical chirality, since the so called chiral components of the nonlinear optical susceptibility also introduce some changes in the polarization charts.

6. Acknowledgment

Authors are grateful to Adriana Passaseo (CNR-NNL-INFM Unità di Lecce) and F. Sarto (Division of Advanced Physics Technologies of ENEA, Roma, Italy) for GaN and ZnO sample preparation, respectively.

7. References

Blachnik R.; Chu J.; Galazka R. R.; Geurts J.; Gutowski J.; Hönerlage B.; Hofmann D.; Kossut J.; Lévy R.; Michler P.; Neukirch U.; Story T.; Strauch D.; Waag A. (1999). Zinc oxide (ZnO). *Landolt-Börnstein-Group III Condensed Matter, Semiconductors: II-VI and I-VII Compounds; Semi-magnetic Compounds*, 41B, 52-53, Springer-Verlag. ISBN: 978-3-540-64964-9

Bloembergen N.; Chang R. K.; Jha S. S. & Lee C. H. (1968). Optical Second-Harmonic Generation in Reflection from Media with Inversion Symmetry. *Physical Review*, Vol.174, No.3, pp. 813-822, ISSN: 0031-899X

Bovino F.A.; Larciprete M.C.; Belardini A.; Sibilia C. (2009). Evaluation of the optical axis tilt of zinc oxide films via noncollinear second harmonic generation. *Applied Physics Letters*, Vol.94, No.25, pp.251109 (3 pages), ISSN: 0003-6951

Cattaneo S. & Kauranen M. (2003). Determination of second-order susceptibility components of thin films by two-beam second-harmonic generation. *Optics Letters*, Vol.28, No.16, pp.1445-1447, ISSN: 0146-9592

Cattaneo S. & Kauranen M. (2005). Polarization-based identification of bulk contributions in nonlinear optics. *Physical Review B* Vol.72, No.3, pp.033412 (4 pages) ISSN 1098-0121

Chen J.; Levine Z.H.; Wilkins J.W. (1995). Calculated second harmonic susceptibilities of BN, AlN, and GaN. *Applied Physics Letters*, Vol.66, No.9, pp. 1129-1131, ISSN: 0003-6951

Clays K.; Van Elshocht S. ; Chi M.; Lepoudre E. & Persoons A. (2001). Bacteriorhodopsin: a natural, efficient (nonlinear) photonic crystal. *Journal of the Optical Society of America B*. Vol.18, No.10, pp.1474-1482, ISSN: 0740-3224

Faccio D.; Pruneri V. & Kazansky P.G. (2000). Noncollinear Maker's fringe measurements of second-order nonlinear optical layers. *Optics Letters*, Vol. 25, No.18, pp.1376-78, ISSN: 0146-9592

Figliozzi P.; Sun L.; Jiang Y.; Matlis N.; Mattern B.; Downer M.C.; Withrow S.P.; White C.W.; Mochán W.L. & Mendoza B.S. (2005). Single-Beam and Enhanced Two-Beam Second-Harmonic Generation from Silicon Nanocrystals by Use of Spatially Inhomogeneous Femtosecond Pulses. *Physical Review Letters*, Vol.94, No.4, pp.047401/1-047401/4, ISSN: 0031-9007

Hecht L. & Barron L.D. (1996). New aspects of second-harmonic optical activity from chiral surfaces and interfaces. *Molecular Physics*, Vol.89, No.1, pp.61-80, ISSN: 0026-8976

Huttunen M.J.; Erkintalo M. & Kauranen M. (2009). Absolute nonlinear optical probes of surface chirality. Journal of Optics A: Pure and Applied Optics, Vo.11, No.3, pp.034006, ISSN: 1464-4258

Jerphagnon J. & Kurtz S.K. (1970). Maker fringes: a detailed comparison of theory and experiment for isotropic and uniaxial crystals. *Journal of Applied Physics*, Vol.41, No.4, pp.1667-1681, ISSN: 0021-8979

Larciprete M.C.; Belardini A.; Sibilia C.; Saab M.-b.; Váró G. & Gergely C. (2010). Optical chirality of bacteriorhodopsin films via second harmonic Maker's fringes measurements. *Applied Physics Letters*, Vol.96, No.22, pp.221108 (3 pages), ISSN: 0003-6951

Larciprete M.C.; Bovino F.A.; Giardina M.; Belardini A.; Centini M.; Sibilia C.; Bertolotti M.; Passaseo A. & Tasco V. (2009). Mapping the nonlinear optical susceptibility by noncollinear second-harmonic generation. *Optics Letters*, Vol.34, No.14, pp.2189-2191, ISSN: 0146-9592

Maker P. D.; Terhune R. W.; Nisenoff M. & Savage C. M. (1962). Effects of Dispersion and Focusing on the Production of Optical Harmonics. *Physical Review Letters*, Vol.8, No.1, pp.21-22, ISSN: 0031-9007

Miragliotta J.; Wickenden D.K.; Kistenmacher T.J. & Bryden W.A (1993). *Journal of the Optical Society of America B,* Vol.10, No.8, pp.1447-1456, ISSN: 0740-3224

Muenchausen R.E.; Keller R.A. & Nogar N.S. (1987). Surface second-harmonic and sum-frequency generation using a noncollinear excitation geometry. *Journal of the Optical Society of America B,*, Vol.4, No.2, pp.237-241, ISSN: 0740-3224

Petralli-Mallow T.; Wong T.M.; Byers J.D.; Lee H.I. & Hicks J.M. (1993). Circular dichroism spectroscopy at interfaces: a surface second harmonic generation study. *Journal of Physical Chemistry,* Vol.97, No.7, pp.1383-1388, ISSN: 0022-3654

Poti B.; Tagliente M.A. & Passaseo A. (2006). *Journal of Non-Crystalline Solids*, Vol.352, No.23, pp.2332-2334, ISSN: 0022-3093

Provencher P.; Côté C.Y. & Denariez-Roberge M.M. (1993). Surface second-harmonic susceptibility determined by noncollinear reflected second-harmonic generation. *Canadian Journal of Physics.*, Vol.71, No.1-2, pp.66-69, ISSN: 0008-4204

Schmidt P. K. & Rayfield G. W. (1994). Hyper-Rayleigh light scattering from an aqueous suspension of purple membrane. *Applied Optics*, Vol.33, No.19, pp.4286-4292, ISSN: 1559-128X

Verbiest T.; Kauranen M.; Maki J.J.; Teerenstra M.N.; Schouten A.J.; Nolte R.J.M. & Persoons A. (1995). Linearly polarized probes of surface chirality. Journal of Chemical Physics, Vol.103, No.18, pp.8296- 8298, ISSN. 0021-9606

Verbiest T.; Kauranen M.; Persoons A.; Ikonen M.; Kurkela J. & Lemmetyinen H. (1994). Nonlinear Optical Activity and Biomolecular Chirality. *Journal of the American Chemical Society*, Vol.116, No.20, pp.9203-9205, ISSN: 0002-7863

Volkov V.; Svirko Yu. P.; Kamalov V. F.; Song L. & El-Sayed M. A. (1997). Optical rotation of the second harmonic radiation from retinal in bacteriorhodopsin monomers in Langmuir-Blodgett film: evidence for nonplanar retinal structure. *Biophysical Journal*, Vol.73, No.6, pp.3164-3170, ISSN: 0006-3495

Weiβenrieder K.S. & Muller J. (1997). Conductivity model for sputtered ZnO-thin film gas sensors. *Thin Solid Films*, Vol.300, No.1-2, pp.30-41, ISSN: 0040-6090

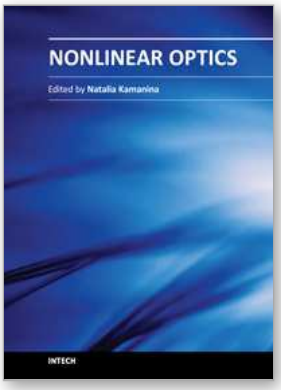

Nonlinear Optics

Edited by Dr. Natalia Kamanina

ISBN 978-953-51-0131-4
Hard cover, 224 pages
Publisher InTech
Published online 29, February, 2012
Published in print edition February, 2012

Rapid development of optoelectronic devices and laser techniques poses an important task of creating and studying, from one side, the structures capable of effectively converting, modulating, and recording optical data in a wide range of radiation energy densities and frequencies, from another side, the new schemes and approaches capable to activate and simulate the modern features. It is well known that nonlinear optical phenomena and nonlinear optical materials have the promising place to resolve these complicated technical tasks. The advanced idea, approach, and information described in this book will be fruitful for the readers to find a sustainable solution in a fundamental study and in the industry approach. The book can be useful for the students, post-graduate students, engineers, researchers and technical officers of optoelectronic universities and companies.

How to reference

In order to correctly reference this scholarly work, feel free to copy and paste the following:

Fabio Antonio Bovino, Maria Cristina Larciprete, Concita Sibilia, Maurizio Giardina, G. Váró and C. Gergely (2012). Nonlinear Ellipsometry by Second Harmonic Generation, Nonlinear Optics, Dr. Natalia Kamanina (Ed.), ISBN: 978-953-51-0131-4, InTech, Available from: http://www.intechopen.com/books/nonlinear-optics/nonlinear-ellipsometry-by-second-harmonic-generation

INTECH
open science | open minds

InTech Europe
University Campus STeP Ri
Slavka Krautzeka 83/A
51000 Rijeka, Croatia
Phone: +385 (51) 770 447
Fax: +385 (51) 686 166
www.intechopen.com

InTech China
Unit 405, Office Block, Hotel Equatorial Shanghai
No.65, Yan An Road (West), Shanghai, 200040, China
中国上海市延安西路65号上海国际贵都大饭店办公楼405单元
Phone: +86-21-62489820
Fax: +86-21-62489821